Journal of Alloys and Compounds 823 (2020) 151769

Contents lists available at ScienceDirect

Journal of Alloys and Compounds

journal homepage: http://www.elsevier.com/locate/jalcom

Integration of VS_2 nanosheets into carbon for high energy density micro-supercapacitor

Waqas Ali Haider [a], Muhammad Tahir [a], Liang He [a, b, *], Wei Yang [a], Aamir Minhas-khan [c], Kwadwo Asare Owusu [a], Yiming Chen [a], Xufeng Hong [a], Liqiang Mai [a, **]

[a] State Key Laboratory of Advanced Technology for Materials Synthesis and Processing, Wuhan University of Technology, Wuhan, 430070, PR China
[b] Department of Materials Science and Nano Engineering, Rice University, Houston, TX, 77005, United States
[c] Department of Electrical Engineering and Computer Science, York University, Toronto, M3J 1P3, Canada

ARTICLE INFO

Article history:
Received 9 September 2018
Received in revised form
7 June 2019
Accepted 8 August 2019
Available online 8 August 2019

Keywords:
Nanosheets
Pyrolyzed carbon
Micro-supercapacitor
Energy density

ABSTRACT

For portable electronics, the development of on-chip micro-supercapacitor (MSC) with high energy density is still a tremendous challenge. Carbon-based microelectrodes are very attractive for applications in MSCs, however, their potential window, porous structure and capacitance need to be enhanced and optimized. Herein, we report a pyrolyzed carbon/vanadium disulfide nanosheets (C/VS_2) microelectrode based MSC by modern micromachining photolithography and pyrolysis process. For this C/VS_2 composite microelectrode, carbon and VS_2 contribute synergistically with gel electrolyte and an improved volumetric capacitance with wide potential window is obtained. The fabricated MSC demonstrates a high specific volumetric capacitance of 86.4 F cm^{-3}, a high energy and a power densities of 15.6 mWh·cm^{-3} and 2.88 W cm^{-3}, respectively with an extended potential window (0–1.2 V). In addition, it shows an excellent cycling behavior, retaining 97.7% capacitance after 10,000 CV cycles at a scan rate of 500 mV s^{-1}. This proposed approach provides a highly promising strategy of fabricating high-performance energy storage devices for miniaturized electronics.

1. Introduction

Supercapacitors (SCs) have gained much consideration due to their exceptional advantages, such as long life, fast charge-discharge and ultrahigh power density [1,2]. The charge storage mechanism of electric double layer capacitors (EDLCs) is mainly due to adsorption and desorption of the ions at electrode/electrolyte interface, while pseudocapacitors can deliver a higher capacitance than that of EDLCs because of their fast and reversible faradaic redox reaction [3–5]. In comparison with EDLCs, the pseudocapacitors usually have shorter cycling life and lower reliability. Therefore, a hybrid SC is developed either by constructing composite exhibiting hybrid charge storage mechanism or using different positive and negative electrodes [6,7]. SCs based on EDLC mechanism have long cycle lifetime as ideally they function without forming chemical bonds or volumetric changes in electrochemically active materials [8,9]. Charge storage at the electrode surface facilitates rapid charge-discharge process and thus superior power capabilities are obtained [10]. Micro-supercapacitors (MSCs) have great potential in portable and miniaturized electronic devices/systems by virtue of their small volume and the ability to store energy in a very short time [11–13]. The design of microelectrodes with high areal and volumetric exploitation of electrochemically active materials is an important factor for obtaining MSCs with high energy and power densities [14].

Low dimensional materials are attracting extensive research interests in electrochemical energy storage applications [15]. Among which, transition metal dichalcogenides (TMDs) are highly promising due to their inimitable layered structure analogous to graphene [16,17]. VS_2 is a representative candidate of TMD family having a metal V layer between two S layers. This 2-dimensional (2D) structure allows fast ion diffusion into the layers and enhances the transport of ions [18]. Also VS_2 has very small band gap partly filled at the Fermi level (E_F) and intriguingly present metallic behavior with high electrical conductivity, high specific surface area and unique mechanical properties [19,20]. Feng et al. reported

* Corresponding author. State Key Laboratory of Advanced Technology for Materials Synthesis and Processing, Wuhan University of Technology, Wuhan, 430070, PR China.
** Corresponding author.
E-mail addresses: hel@whut.edu.cn (L. He), mlq518@whut.edu.cn (L. Mai).

https://doi.org/10.1016/j.jallcom.2019.151769
0925-8388/

an in-plane supercapacitor by assembling ultrathin VS_2 nanosheets, delivering a capacitance of 4760 μF cm^{-2} with a remarkable cycling performance [21]. Furthermore, hybrid devices have been explored to work at extended potential difference to obtain improved energy density of SCs. Rantho et al. studied the electrochemical performance of VS_2/C—Fe/PANI hybrid supercapacitor performing at an operating electrode potential of 1.7 V and it exhibited energy density (27.8 Wh·kg^{-1}) and power density (2991.5 W kg^{-1}) [22]. Hybridization of TMDs with carbonaceous materials can improve the performance of carbon by providing more active sites and fast electron transport [23—27].

For carbon materials applied in MSCs, photoresist-derived carbon is highly attractive due to its properties resembling with those of activated carbon and is easy micropatterning for on-chip integration by modern semiconductor microfabrication process. Carbon microelectromechanical system (C-MEMS) is a distinctive approach for fabrication of high-performance pyrolyzed carbon microelectrodes and is highly adequate and compatible with current microtechnologies [28—30]. Researchers have investigated photoresist-derived carbon for high-performance MSCs [31—33]. The electrochemical potential window of pyrolyzed carbon could be enlarged by compositing with high-performance embedded micro/nanostructures of VS_2 and the reliability of active electrode is enhanced [34,35]. Recently, MoS_2@rGO/CNT/pyrolyzed carbon-based MSC is developed, delivering capacitance of 40 F cm^{-3} and an energy density of 5.6 mWh·cm^{-3} [28].

In this work, we studied the all solid-state on-chip MSC with a high energy density at a wide working potential window. Herein, a photoresist/VS_2 composite is micropatterned and pyrolyzed in nitrogen atmosphere to fabricate the interdigital C/VS_2 microelectrodes. The fabricated MSC is measured employing H_2SO_4/PVA gel electrolyte at an extended working potential of 0—1.2 V. This C/VS_2 microelectrode based MSC (C/VS_2-MSC) shows an improved areal capacitance of 9.76 mF cm^{-2} [29,31,32] and a high specific volumetric capacitance of 86.4 F cm^{-3}, enhanced energy density of 15.6 mWh·cm^{-3} and outstanding cycling performance, retaining 97.7% of its initial capacitance even after 10,000 cycles at a scan rate of 0.5 V^{-1}.

2. Experimental

2.1. Synthesis of VS_2 nanosheets

The VS_2 nanosheets were prepared *via* a facile hydrothermal reaction of ammonium metavanadate (NH_4VO_3) and thioacetamide (TAA) [36]. In a typical synthesis, 0.23 g NH_4VO_3 was vigorously dispersed in a mixture of 30 ml deionized (DI) water and 2 mL NH_4OH. Then, 1.12 g TAA was added in the mixture, followed by continuous stirring for 60 min at room temperature. The solution was then sealed into a Teflon-lined autoclave and reserved at 180 °C for 20 h. Afterwards, the sample was cooled down and centrifuged to collect black precipitate, followed by washing with DI water and ethanol. The product was dried in vacuum at 60 °C for 8 h and gently ground with an agate mortar and pestle to obtain the VS_2 nanosheets.

2.2. Materials characterization

To observe the morphology of samples, field emission SEM images were acquired by JEOL JSM-7100 microscope. X-ray diffraction (XRD) were conducted on Bruker D8 Advance X-ray diffractometer with a non-monochromatic Cu Kα X-ray source (λ = 1.5418 Å). Transmission electron microscopic (TEM) and high resolution TEM (HRTEM) images were acquired by JEM-2100F microscope. Raman spectra were obtained by Renishaw RM-1000 laser Raman microscopy system. Thermogravimetric analysis (TGA) was performed at Netzsch STA 449C simultaneous thermal analyzer under nitrgogen atmosphere. X-ray photoelectron spectroscopic (XPS) spectra were collected on VG Multilab 2000 instrument.

2.3. Microfabrication of C/VS_2-MSC and electrochemical measurements

The C-MEMS technique is employed for microfabrication of C/VS_2-MSC. The procedure of microfabrication is schematically illustrated in Fig. 1. For the preparation of photoresist/VS_2 composite, 0.05 g VS_2 was mixed with 0.95 g PR1-9000A photoresist and 10 droplets of SD1 solvent diluents (Futurrex, Inc., Co., Ltd.) by constant stirring and ultrasonication for 10 h. The flask containing mixture was kept in vacuum for 120 min to eliminate the trapped bubbles. Meanwhile, Si/SiO_2 substrate with 300 nm thick SiO_2 layer was cleaned by a typical RCA cleaning process and dehydrated at 145 °C for 15 min. Then the homogenous photoresist/VS_2 composite was spin-coated on Si/SiO_2 substrate at 1000 rpm for 10 s and then 6000 rpm for 40 s. Afterwards, the samples were pre-baked at 100 °C for 15 min. Optimized photolithography was carried out, followed by development with RD6 developer and rinse to obtain the interdigital micropattern with 8 in-plan fingers. Fine micropattern of photresist/VS_2 composite was achieved, as shown in the optical image of Fig. S1(a) (supplementary information). The samples were baked at 115 °C for 15 min and then annealed in a quartz tube furnace under nitrogen flow. Initially the samples were reserved at 400 °C for 1 h, then the temperature raised to 900 °C with a heating rate of 2 °C·min^{-1} and remained at 900 °C for 60 min, at last cooled down naturally. Photoresist/VS_2 was pyrolyzed to obtain C/VS_2 microelectrodes. The composite has weight loss and volume shrinkage after carbonization. The optical image of fine patterned C/VS_2 microelectrodes shows practicability of the fabrication process as there are no defects or cracks in the microelectrodes Fig. S1(b). The detailed dimensions of micropattern are shown in Fig. S2, having 4 fingers per polarity and the size of each finger is 0.26 cm × 0.04 cm with a finger gap of 0.01 cm (area of microelectrodes is 0.1066 cm^2).

The electrochemical measurements of the MSCs were carried out by conducting cyclic voltammetry (CV), galvanostatic charge-discharge (GCD), and electrochemical impedance spectroscopy (EIS) with two-electrode system using Autolab 302 N. Based on the analysis of IR drop, the equivalent series resistance (*ESR*) is calculated by equation (1) as follows [37]:

$$ESR = \frac{V_{drop}}{2 \cdot I} A \tag{1}$$

where V_{drop} is the IR drop, and A is the area of electrodes. I represents the current.

Furthermore, by using the results of GCD curves, the specific volumetric capacitance (C_v), volumetric energy density (E_v) and power density (P_v) of the C/VS_2-MSC are evaluated using following equations (2)–(4) [38,39].

$$C_v = \frac{I \Delta t}{v \Delta V} \tag{2}$$

$$E_v = \frac{1}{2} C_v \cdot (\Delta V)^2 \tag{3}$$

$$P_v = \frac{E_v}{\Delta t} \tag{4}$$

where I is the GCD current, and operating potential window is

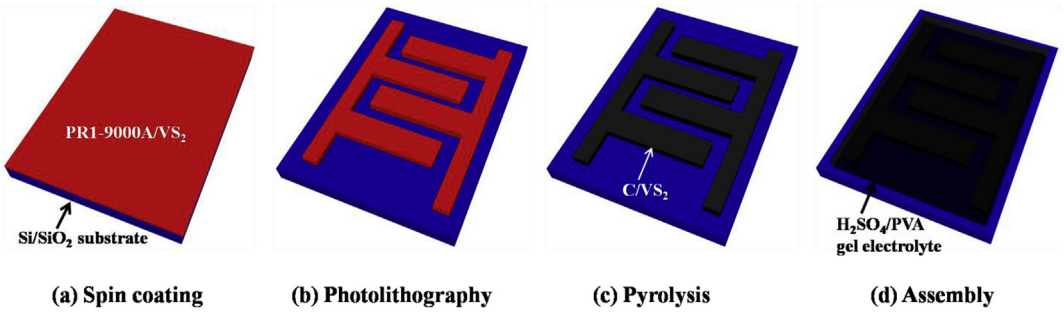

Fig. 1. Schematic illustration of microfabrication process of C/VS_2-MSC.

represented by ΔV. Δt is the discharge time, and v is the volume of microelectrodes.

3. Results and discussions

The morphology and microstructure of VS_2 nanosheets were observed by SEM. Fig. 2(a) clearly shows that 50–100 nm thick VS_2 nanosheets are assembled to form the flower-like structures. The energy-dispersive spectroscopy (EDS) mapping result of VS_2 nanosheets is shown in Fig. S3 confirming the presence and homogenous distribution of V and S with a ratio of 1:2. Fig. 2(b) presents the SEM image of patterned C/VS_2 microelectrodes, here we can clearly observe that the VS_2 is embedded and uniformly dispersed in pyrolyzed carbon. The inset shows a magnified image of one VS_2 structure and we can observe that VS_2 preserves its nanosheets assembled flower-like structure. The EDS mapping of the C/VS_2 is described in Fig. S4, that also confirms the subsistence of V, S and C elements, while O comes from SiO_2 substrate. The SEM image of surface of C/VS_2 microelectrode is shown in Fig. S5(a), and the thickness of microelectrode was measured by cross-section SEM image and calculated to be 1.13 μm, as shown in Fig. S5(b).

The VS_2 and C/VS_2 were characterized by XRD for phase analysis (Fig. 2(c)). The peaks in their XRD patterns are in accordance with the standard peaks of hexagonal VS_2 (JCPDS Card No 01-089-1640). The XRD pattern of C/VS_2 shows a wide peak centered at 15° that corresponds to the amorphous carbon [40]. TEM and HRTEM measurements were taken to investigate fine structures in VS_2 nanosheets and C/VS_2 composite (Fig. 2(d), (e)). HRTEM image displays an interplaner spacing of 0.25 nm, which corresponds to (011) crystal plane and XRD peak at 35.7° of hexagonal phase of VS_2. Fig. 2(f) shows the Raman spectroscopy of C/VS_2 microelectrode and the result verifies the carbonaceous nature of pyrolyzed material. Disorder-induced band (D-band) and graphitic band (G-band) can be observed at 1320 and 1600 cm^{-1}, respectively, with corresponding small intensity ratio of D and G band ($I_D/I_G = 0.99$) [41].

Thermogravimetric analysis of PR1-9000A and VS_2 nanosheets was conducted in nitrogen atmosphere. Fig. 3(a) demonstrates a typical TGA curve, showing 55.8% and 78.4% weight retention of PR1-9000A and VS_2 nanosheets at 900 °C, respectively. As presented in Fig. 3 (b), (c) and (d), XPS characterization was performed to measure the estimated valence states of elements on the surface of C/VS_2 microelectrode. The spectra reveal the presence of V, S and C elements in the C/VS_2 microelectrode. The C 1s peak at 284.7 eV is attributed to the occurrence of non-oxidized sp^2 C. The V 2p peaks centered at 515.9 and 523.4 eV are indexed to V $2p_{3/2}$ and V $2p_{1/2}$, indicating a V valence of +4. In S 2p core level, two characteristic

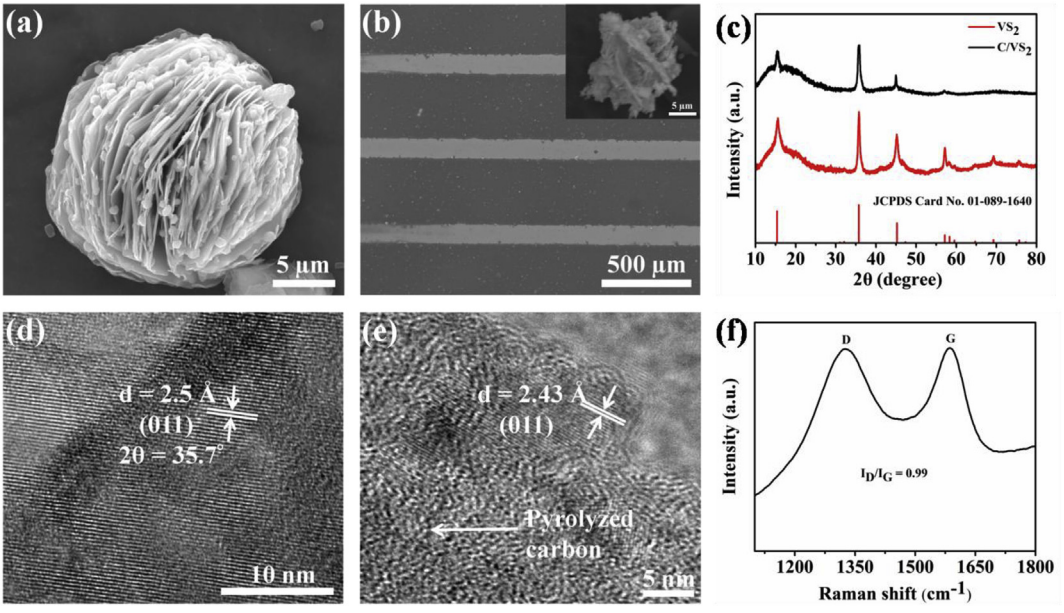

Fig. 2. (a) SEM image of the synthesized VS_2 nanosheets with layered structure. (b) SEM image of micropatterned C/VS_2 microelectrodes, inset is the SEM image of microstructure of VS_2 embedded in pyrolyzed carbon. (c) XRD patterns of VS_2 nanosheets and C/VS_2 microelectrodes. (d) TEM image of VS_2 nanosheets. (e) HRTEM image of C/VS_2 composite, (f) Raman spectrum of C/VS_2 microelectrode.

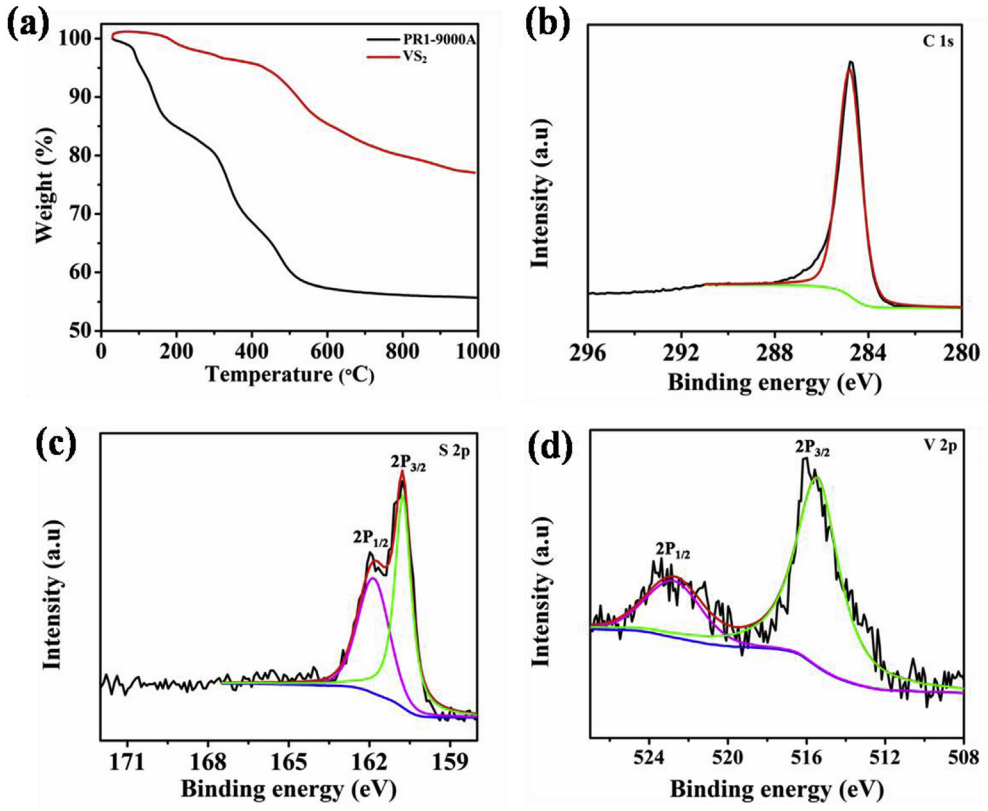

Fig. 3. (a) TGA curves of VS_2 nanosheets and PR1-9000A photoresist, (b), (c) and (d) XPS spectra indicating C 1s, S 2p, and V 2p core levels of C/VS_2 microelectrodes.

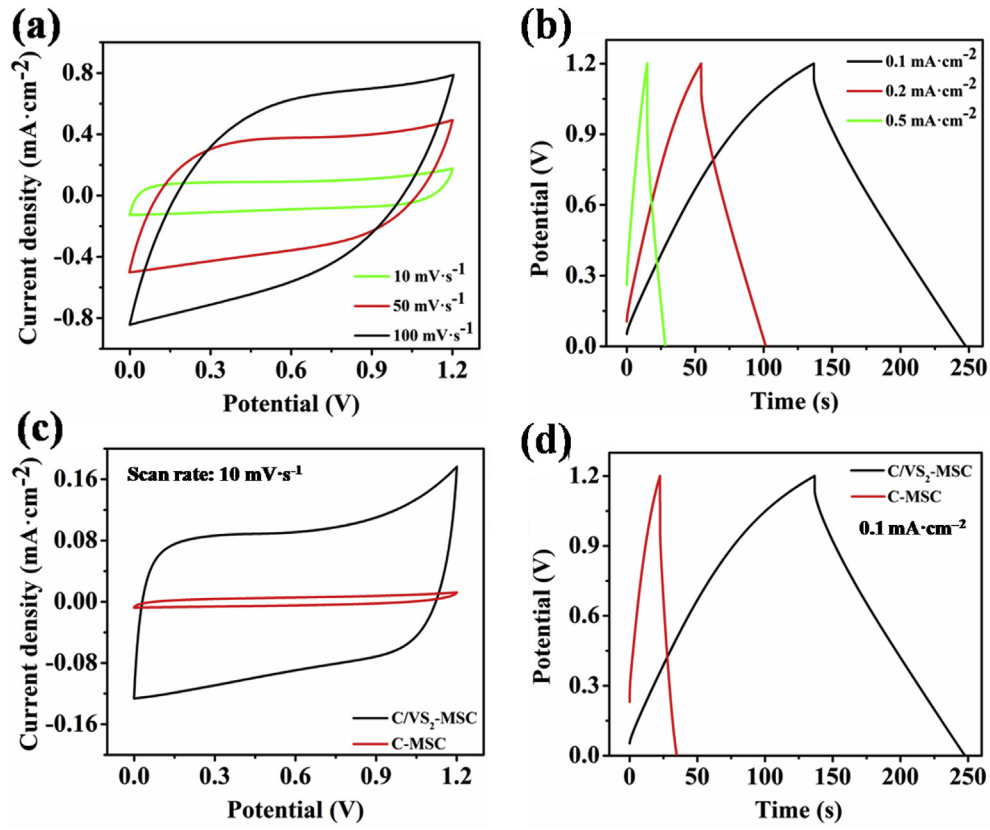

Fig. 4. (a) CV curves of C/VS_2-MSC at various scan rates. (b) GCD curves of the C/VS_2-MSC at various current densities. (c) and (d) comparison of CV and GCD curves of C/VS_2-MSC and C-MSC.

peaks at the binding energies of 160.6 eV for S $2p_{3/2}$ and 161.9 eV for S $2p_{1/2}$ confirms the presence of the S^{2-} in the C/VS_2 microelectrode [24,42].

The electrochemical performance of C/VS_2-MSC was investigated by CV, GCD and EIS measurements with two-electrodes system, and 1 M PVA/H_2SO_4 gel electrolyte was employed. Fig. 4(a) presents the quasi rectangular CV curves of C/VS_2-MSC at different scan rates. The accumulation of charges and the rapid reversible electron-exchange reactions at the electrode/electrolyte interface refers to a hybrid type SC [43]. The quasi symmetrical triangular charge/discharge curves reveal the capacitive nature due to existence of EDLC and faradaic behavior, in accordance with the CV curves, as indicated in Fig. 4(b). The GCD curve shows the long charge/discharge time and a small IR drop of 0.062 V at current density of 0.1 mA cm^{-2}. The CV and GCD curves of C/VS_2-MSC and pyrolyzed carbon based MSC (C-MSC) are evaluated and presented in Fig. 4(c), (d). The current density of C/VS_2-MSC is superior to that of C-MSC at a scan rate of 10 mV s^{-1}, showing greater capacitive properties. The GCD curves at a current density of 0.1 mA cm^{-2} demonstrate significant improvement in electrochemical performance. As calculated from GCD curve, C/VS_2-MSC exhibits a specific capacitance of 86.4 F cm^{-3} at a current density of 0.1 mA cm^{-2} which is much higher than that of C-MSC (11 F cm^{-3}). Moreover, using the IR drop, the ESR of C/VS_2 is estimated to be ~314 Ω cm^2. Considering that there are no conductive additives into the C/VS_2 microelectrodes, we believe that the smaller ESR of C/VS_2 than that of carbon microelectrodes could be ascribed to the high electrical conductivity of metallic VS_2 nanosheets.

Fig. 5(a) exhibits the comparison of specific capacitances of C/VS_2-MSC and C-MSC evaluated from the GCD curves acquired at different current densities. With the increase of current density, the capacitance continuously decreases. At high current density, ions have insufficient time to diffuse or adsorb at the electrode/electrolyte interfaces, so the capacitance will decrease. The C/VS_2 has a higher volumetric specific capacitance than that of C-MSC and shows a rate capability of 58.4% of capacitance retention at 1 mA cm^{-2} compared with that at 0.1 mA cm^{-2}.

To further investigate the impedance of C/VS_2-MSC and C-MSC, EIS test was conducted in a frequency of 100 kHz to 0.01 Hz, as given in Fig. 5(b). The intercept at real axis reveals the lower ESR of C/VS_2-MSC, since its electrical conductivity is higher than that of C-MSC. The sheer graph with steep slope in Warburg region (low frequency) displays the ion mobility and diffusion in the microelectrodes resulting in improved electrochemical performance [44].

In addition, the C/VS_2-MSC also shows the excellent cycling performance that is of much significance for its practical applications. 97.7% of initial capacitance is retained even after 10,000 CV cycles at scan rate of 0.5 V s^{-1} (Fig. 5(c)). A minor loss of 2.3% in capacitance could be attributed to short diffusion pathway for electrolyte ions, enhanced reaction reversibility, reduced number of defect sites, and high surface area of the porous carbon [45,46]. We also performed voltage holding stability test at a constant voltage of 1.2 V for 200 h. Three charge/discharge cycles from 0 to 1.2 V were carried out every 10 h at a current density of 0.1 mA cm^{-2} to quantify the corresponding capacitance retention. C/VS_2-MSC

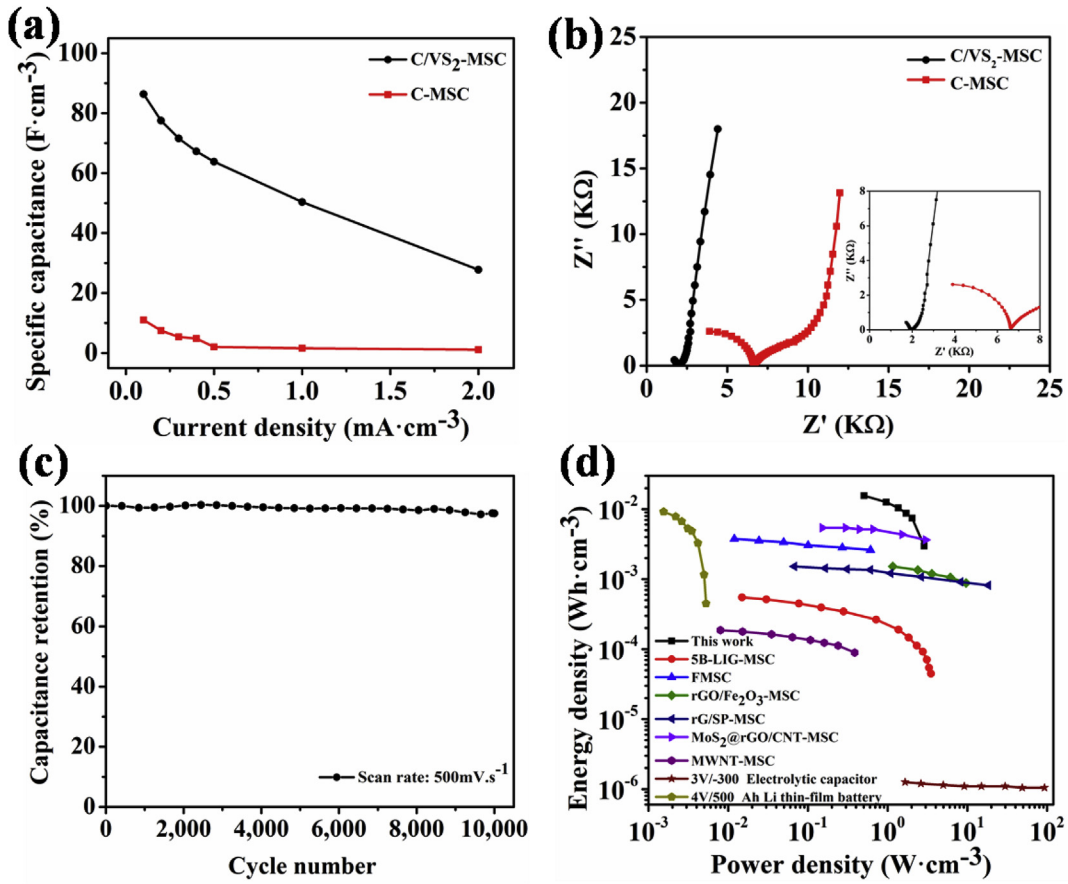

Fig. 5. (a) Specific volumetric capacitances of C/VS_2-MSC and C-MSC at various current densities. (b) Nyquist plots of C/VS_2-MSC and C-MSC, inset is the Nyquist plot in high-frequency region. (c) Cycling performance of C/VS_2-MSC at scan rate of 0.5 V s^{-1}. (d) Ragone plot of the C/VS_2-MSC, and comparison with recently reported TMD-based MSCs, carbon-based MSCs and conventional storage devices.

displays exceptional stability with negligible loss of capacitance, as shown in Fig. S6 (Supporting Information). Furthermore, the high stability of microelectrodes reveals that the charge transfer reaction is reversible [47].

The evaluation of energy density and power density is desirable for practical applications of energy storage devices [48,49]. C/VS_2-MSC shows an energy density of 15.6 mWh·cm^{-3} and power density of 2.95 W cm^{-3}, evaluated from GCD curves in a potential window of 0–1.2 V, which are superior to recently reported TMD and carbon-based MSCs, such as core-sheath carbon fibers MSC with 3.75 mWh·cm^{-3} and 612 mW cm^{-3} [39]. Recently reported MoS_2@rGO/CNT-MSC delivered energy density of 5.6 mWh·cm^{-3}, MWNT-MSC and rGO/Fe_2O_3-MSC displayed 0.18 mWh·cm^{-3}, 1.61 mWh·cm^{-3} and maximum power density of 0.4 W cm^{-3} and 9.82 W cm^{-3}, respectively [50,51]. Fig. 5(d) presents the Ragone plot comparing the volumetric energy and power densities of this work to some MSCs recently developed [52–54]. A comparison of electrochemical performances of on-chip MSCs is presented in Table 1 (Supporting Information). The high performance is mainly resulted from the high capacitive properties of VS_2, high-surface-area porous carbon, larger potential window and fine microelectrodes with controlled narrow gaps between interdigital fingers.

4. Conclusions

In summary, we synthesized microflower structures of layered VS_2 nanosheets through facile hydrothermal method. An all-solid-state C/VS_2-MSC is fabricated by optimized photolithography and pyrolysis. The layered VS_2 nanosheets embedded in pyrolyzed carbon provide more active sites for ion diffusion and charge storage, thus the synergistic contribution of carbon and VS_2 leads to a high volumetric specific capacitance (86.4 F cm^{-3}), and high energy density (15.6 mWh·cm^{-3}) in a wide operating potential window (0–1.2 V) with an outstanding cycling performance. The proposed approach provides feasibility for layered TMDs to be developed and applied in carbon-based MSCs to realize high energy and power densities.

Acknowledgements

This work was supported by the National Natural Science Fund for Distinguished Young Scholars (51425204), the National Natural Science Foundation of China (51521001, 51579198), the National Key Research and Development Program of China (2016YFA0202603, 2016YFA0202604), the Programme of Introducing Talents of Discipline to Universities (B17034), the Yellow Crane Talent (Science & Technology) Program of Wuhan City, and the Wuhan Morning Light Plan of Youth Science and Technology (No. 2017050304010316).

Appendix A. Supplementary data

Supplementary data to this article can be found online at https://doi.org/10.1016/j.jallcom.2019.151769.

References

[1] Y.-W. Chi, C.-C. Hu, H.-H. Shen, K.-P. Huang, New approach for high-voltage electrical double-layer capacitors using vertical graphene nanowalls with and without nitrogen doping, Nano Lett. 16 (2016) 5719–5727.
[2] L. Qu, Y. Zhao, A.M. Khan, C. Han, K.M. Hercule, M. Yan, X. Liu, W. Chen, D. Wang, Z. Cai, Interwoven three-dimensional architecture of cobalt oxide nanobrush-graphene@ $Ni_xCo_{2x}(OH)_{6x}$ for high-performance supercapacitors, Nano Lett. 15 (2015) 2037–2044.
[3] H. Jiang, P.S. Lee, C. Li, 3D carbon based nanostructures for advanced supercapacitors, Energy Environ. Sci. 6 (2013) 41–53.
[4] S. Park, S.-W. Kang, K. Kim, Competition between ionic adsorption and desorption on electrochemical double layer capacitor electrodes in acetonitrile solutions at different currents and temperatures, J. Power Sources 372 (2017) 8–15.
[5] V. Augustyn, P. Simon, B. Dunn, Pseudocapacitive oxide materials for high-rate electrochemical energy storage, Energy Environ. Sci. 7 (2014) 1597–1614.
[6] S.-B. Ma, K.-W. Nam, W.-S. Yoon, X.-Q. Yang, K.-Y. Ahn, K.-H. Oh, K.-B. Kim, A novel concept of hybrid capacitor based on manganese oxide materials, Electrochem. Commun. 9 (2007) 2807–2811.
[7] Y.-G. Wang, L. Cheng, Y.-Y. Xia, Electrochemical profile of nano-particle CoAl double hydroxide/active carbon supercapacitor using KOH electrolyte solution, J. Power Sources 153 (2006) 191–196.
[8] J.P. Alper, S. Wang, F. Rossi, G. Salviati, N. Yiu, C. Carraro, R. Maboudian, Selective ultrathin carbon sheath on porous silicon nanowires: materials for extremely high energy density planar micro-supercapacitors, Nano Lett. 14 (2014) 1843–1847.
[9] E. Frackowiak, F. Beguin, Carbon materials for the electrochemical storage of energy in capacitors, Carbon 39 (2001) 937–950.
[10] H. Ji, X. Zhao, Z. Qiao, J. Jung, Y. Zhu, Y. Lu, L.L. Zhang, A.H. MacDonald, R.S. Ruoff, Capacitance of carbon-based electrical double-layer capacitors, Nat. Commun. 5 (2014) 3317.
[11] D. Yu, K. Goh, Q. Zhang, L. Wei, H. Wang, W. Jiang, Y. Chen, Controlled functionalization of carbonaceous fibers for asymmetric solid-state micro-supercapacitors with high volumetric energy density, Adv. Mater. 26 (2014) 6790–6797.
[12] X. Dong, Z. Guo, Y. Song, M. Hou, J. Wang, Y. Wang, Y. Xia, Flexible and wire-shaped micro-supercapacitor based on $Ni(OH)_2$-Nanowire and ordered mesoporous carbon electrodes, Adv. Funct. Mater. 24 (2014) 3405–3412.
[13] L. Mai, X. Tian, X. Xu, L. Chang, L. Xu, Nanowire electrodes for electrochemical energy storage devices, Chem. Rev. 114 (2014) 11828–11862.
[14] X. Tian, M. Shi, X. Xu, M. Yan, L. Xu, A. Minhas-Khan, C. Han, L. He, L. Mai, Arbitrary shape engineerable spiral micropseudocapacitors with ultrahigh energy and power densities, Adv. Mater. 27 (2015) 7476–7482.
[15] B. Liu, L.-J. Wu, Y.-Q. Zhao, L.-Z. Wang, M.-Q. Cai, A first-principles study of magnetic variation via doping vacancy in monolayer VS_2, J. Magn. Magn. Mater. 420 (2016) 218–224.
[16] Y. Zhang, X. Wu, Vanadium sulfide nanoribbons: electronic and magnetic properties, Phys. Lett. A 377 (2013) 3154–3157.
[17] M. Zhong, Y. Li, Q. Xia, X. Meng, F. Wu, J. Li, Ferromagnetism in VS_2 nanostructures: nanoflowers versus ultrathin nanosheets, Mater. Lett. 124 (2014) 282–285.
[18] J. Zhou, L. Wang, M. Yang, J. Wu, F. Chen, W. Huang, N. Han, H. Ye, F. Zhao, Y. Li, Hierarchical VS_2 nanosheet assemblies: a universal host material for the reversible storage of alkali metal ions, Adv. Mater. 29 (2017) 1702061.
[19] Q. Ji, C. Li, J. Wang, J. Niu, Y. Gong, Z. Zhang, Q. Fang, Y. Zhang, J. Shi, L. Liao, Metallic vanadium disulfide nanosheets as a platform material for multifunctional electrode applications, Nano Lett. 17 (2017) 4908–4916.
[20] L. Fang, Z. Zhang, X. Li, H. Zhou, K. Ma, L. Ge, K. Huang, Fabrication of hybrid cauliflower-like nanoarchitectures by in situ grown ZnO nanoparticals on VS_2 ultrathin nanosheets for high performance supercapacitors, Colloid. Surf. Physicochem. Eng. Asp. 501 (2016) 42–48.
[21] J. Feng, X. Sun, C. Wu, L. Peng, C. Lin, S. Hu, J. Yang, Y. Xie, Metallic few-layered VS_2 ultrathin nanosheets: high two-dimensional conductivity for in-plane supercapacitors, J. Am. Chem. Soc. 133 (2011) 17832–17838.
[22] M. Rantho, M. Madito, F. Ochai-Ejeh, N. Manyala, Asymmetric supercapacitor based on vanadium disulfide nanosheets as a cathode and carbonized iron cations adsorbed onto polyaniline as an anode, Electrochim. Acta 260 (2018) 11–23.
[23] P. Mohan, J. Yang, A. Jena, H.S. Shin, VS_2/rGO hybrid nanosheets prepared by annealing of VS_4/rGO, J. Solid State Chem. 224 (2015) 82–87.
[24] C.S. Rout, B.-H. Kim, X. Xu, J. Yang, H.Y. Jeong, D. Odkhuu, N. Park, J. Cho, H.S. Shin, Synthesis and characterization of patronite form of vanadium sulfide on graphitic layer, J. Am. Chem. Soc. 135 (2013) 8720–8725.
[25] Y. Li, H. Wang, L. Xie, Y. Liang, G. Hong, H. Dai, MoS_2 nanoparticles grown on graphene: an advanced catalyst for the hydrogen evolution reaction, J. Am. Chem. Soc. 133 (2011) 7296–7299.
[26] K. Chang, W. Chen, L-cysteine-assisted synthesis of layered MoS_2/graphene composites with excellent electrochemical performances for lithium ion batteries, ACS Nano 5 (2011) 4720–4728.
[27] Q. Xiang, J. Yu, M. Jaroniec, Synergetic effect of MoS_2 and graphene as cocatalysts for enhanced photocatalytic H_2 production activity of TiO_2 nanoparticles, J. Am. Chem. Soc. 134 (2012) 6575–6578.
[28] W. Yang, L. He, X. Tian, M. Yan, H. Yuan, X. Liao, J. Meng, Z. Hao, L. Mai, Carbon-mems-based alternating stacked MoS_2@rGO-CNT micro-supercapacitor with high capacitance and energy density, Small 13 (2017) 1700639.
[29] B. Hsia, M.S. Kim, M. Vincent, C. Carraro, R. Maboudian, Photoresist-derived porous carbon for on-chip micro-supercapacitors, Carbon 57 (2013) 395–400.
[30] C. Shen, X. Wang, W. Zhang, F. Kang, Direct prototyping of patterned nanoporous carbon: a route from materials to on-chip devices, Sci. Rep. 3 (2013) 2294.
[31] C. Yin, L. He, Y. Wang, Z. Liu, G. Zhang, K. Zhao, C. Tang, M. Yan, Y. Han, L. Mai, Pyrolyzed carbon with embedded NiO/Ni nanospheres for applications in microelectrodes, RSC Adv. 6 (2016) 43436–43441.
[32] Y. Yang, L. He, C. Tang, P. Hu, X. Hong, M. Yan, Y. Dong, X. Tian, Q. Wei, L. Mai, Improved conductivity and capacitance of interdigital carbon microelectrodes through integration with carbon nanotubes for micro-supercapacitors, Nano

Res. 9 (2016) 2510–2519.
[33] X. Hong, L. He, X. Ma, W. Yang, Y. Chen, L. Zhang, H. Yan, Z. Li, L. Mai, Microstructuring of carbon/tin quantum dots via a novel photolithography and pyrolysis-reduction process, Nano Res. 10 (2017) 3743–3753.
[34] G.Z. Chen, Understanding supercapacitors based on nano-hybrid materials with interfacial conjugation, Pro. Nat. Sci. Mater. 23 (2013) 245–255.
[35] M. Tahir, L. He, W.A. Haider, W. Yang, X. Hong, Y. Guo, X. Pan, H. Tang, Y. Li, L. Mai, Co-electrodeposited porous PEDOT-CNT microelectrodes for integrated micro-supercapacitor with high energy density, high rate capability, and long cycling life, Nanoscale 11 (2019) 7761–7770.
[36] P. He, M. Yan, G. Zhang, R. Sun, L. Chen, Q. An, L. Mai, Layered VS_2 nanosheet-based aqueous Zn ion battery cathode, Adv. Energy Mater. 7 (2017) 1601920.
[37] M.S. Kim, B. Hsia, C. Carraro, R. Maboudian, Flexible micro-supercapacitors with high energy density from simple transfer of photoresist-derived porous carbon electrodes, Carbon 74 (2014) 163–169.
[38] X.C. Tian, B. Xiao, X. Xu, L. Xu, Z.H. Liu, Z.Y. Wang, M.Y. Yan, Q.L. Wei, L.Q. Mai, Vertically stacked holey graphene/polyaniline heterostructures with enhanced energy storage for on-chip micro-supercapacitors, Nano Res. 9 (2016) 1012–1021.
[39] S. Zhai, H.E. Karahan, L. Wei, X. Chen, Z. Zhou, X. Wang, Y. Chen, Hydrothermal assembly of micro-nano-integrated core-sheath carbon fibers for high-performance all-carbon micro-supercapacitors, Energy Storage Mater. 9 (2017) 221–228.
[40] P. Zhou, X. Yang, L. He, Z. Hao, W. Luo, B. Xiong, X. Xu, C. Niu, M. Yan, L. Mai, The Young's modulus of high-aspect-ratio carbon/carbon nanotube composite microcantilevers by experimental and modeling validation, Appl. Phys. Lett. 106 (2015) 111908.
[41] H. Wang, C. Peng, J. Zheng, F. Peng, H. Yu, Design, synthesis and the electrochemical performance of MnO_2/C@CNT as supercapacitor material, Mater. Res. Bull. 48 (2013) 3389–3393.
[42] X. Sun, T. Yao, Z. Hu, Y. Guo, Q. Liu, S. Wei, C. Wu, In situ unravelling structural modulation across the charge-density-wave transition in vanadium disulfide, Phys. Chem. Chem. Phys. 17 (2015) 13333–13339.
[43] T.M. Masikhwa, F. Barzegar, J.K. Dangbegnon, A. Bello, M.J. Madito, D. Momodu, N. Manyala, Asymmetric supercapacitor based on VS_2 nanosheets and activated carbon materials, RSC Adv. 6 (2016) 38990–39000.
[44] X. Ma, S. Feng, L. He, M. Yan, X. Tian, Y. Li, C. Tang, X. Hong, L. Mai, Rapid, all dry microfabrication of three-dimensional Co_3O_4/Pt nanonetworks for high-performance microsupercapacitors, Nanoscale 9 (2017) 11765–11772.
[45] K.M. Hercule, Q. Wei, A.M. Khan, Y. Zhao, X. Tian, L. Mai, Synergistic effect of hierarchical nanostructured MoO_2/$Co(OH)_2$ with largely enhanced pseudocapacitor cyclability, Nano Lett. 13 (2013) 5685–5691.
[46] A. Saha, P. Bharmoria, A. Mondal, S.C. Ghosh, S. Mahanty, A.B. Panda, Generalized synthesis and evaluation of formation mechanism of metal oxide/sulphide@C hollow spheres, J. Mater. Chem. 3 (2015) 20297–20304.
[47] S. Wang, B. Hsia, C. Carraro, R. Maboudian, High-performance all solid-state micro-supercapacitor based on patterned photoresist-derived porous carbon electrodes and an ionogel electrolyte, J. Mater. Chem. 2 (2014) 7997–8002.
[48] L.-Q. Mai, A. Minhas-Khan, X. Tian, K.M. Hercule, Y.-L. Zhao, X. Lin, X. Xu, Synergistic interaction between redox-active electrolyte and binder-free functionalized carbon for ultrahigh supercapacitor performance, Nat. Commun. 4 (2013) 2923.
[49] K.A. Owusu, L. Qu, J. Li, Z. Wang, K. Zhao, C. Yang, K.M. Hercule, C. Lin, C. Shi, Q. Wei, Low-crystalline iron oxide hydroxide nanoparticle anode for high-performance supercapacitors, Nat. Commun. 8 (2017) 14264.
[50] L. Liu, D. Ye, Y. Yu, L. Liu, Y. Wu, Carbon-based flexible micro-supercapacitor fabrication via mask-free ambient micro-plasma-jet etching, Carbon 111 (2017) 121–127.
[51] S. Gu, Z. Lou, L. Li, Z. Chen, X. Ma, G. Shen, Fabrication of flexible reduced graphene oxide/Fe_2O_3 hollow nanospheres based on-chip micro-supercapacitors for integrated photodetecting applications, Nano Res. 9 (2016) 424–434.
[52] Z. Peng, R. Ye, J.A. Mann, D. Zakhidov, Y. Li, P.R. Smalley, J. Lin, J.M. Tour, Flexible boron-doped laser-induced graphene microsupercapacitors, ACS Nano 9 (2015) 5868–5875.
[53] B. Song, L. Li, Z. Lin, Z.-K. Wu, K.-s. Moon, C.-P. Wong, Water-dispersible graphene/polyaniline composites for flexible micro-supercapacitors with high energy densities, Nano Energy 16 (2015) 470–478.
[54] Z.S. Wu, K. Parvez, X. Feng, K. Müllen, Graphene-based in-plane micro-supercapacitors with high power and energy densities, Nat. Commun. 4 (2013) 2487.